



# A predictive model for cortical bone temperature distribution during drilling

Yahui Hu<sup>1</sup> · Hao Ding<sup>1</sup> · Yutao Shi<sup>1</sup> · Huaiyu Zhang<sup>1</sup> · Qingchun Zheng<sup>1,2</sup>

Received: 8 June 2020 / Accepted: 15 December 2020 / Published online: 18 January 2021  
© Australasian College of Physical Scientists and Engineers in Medicine 2021

## Abstract

Bone drilling is an important procedure in medical orthopedic surgery and it is inevitable that heat will be generated during the drilling process and higher temperatures can cause thermal damage to the bone tissue near the drilled hole. Therefore, the capability to obtain the cortical bone drilling temperature distribution area can have great significance for medical bone surgery. Based on the theory of heat transfer, a predictive model for cortical bone drilling temperature distribution was established. The energy distribution coefficient in cortical bone drilling was derived, based on conjugate gradient inversion. A cortical bone drilling experiment platform was built to verify the temperature distribution prediction model. The results show that the model of cortical bone drill temperature distribution could predict accurately the drilling temperature distribution, both for different depths and for different radial distances. Additionally, the effects of different drilling conditions (spindle speed, feed rate, drill diameter) on the temperature of drilling cortical bone were considered.

**Keywords** Predictive model · Cortical bone · Drilling temperature distribution · Heat source method

## Introduction

Bone drilling has become a basic clinical practice in medical orthopedic surgery [1, 2]. In recent years, research into the effects of bone drilling have attracted widespread attention, including the study of material properties of cortical bone/cancellous bone, the construction of bone mechanical models, appraisals of the dynamic mechanical change of bone during drilling, studies of the drilling process in simulated cortical bone and the analysis of the surface quality of bone hole cracks after drilling. An important aspect of the research is the heat distribution during the drilling process [3]. Drilling heat is one of the most important factors

affecting the initial recovery of bone tissue [4–6], and drilling temperature will affect postoperative recovery.

Common methods for measuring bone drilling temperature are the infrared camera method [3, 7–10] and the thermocouple method [11]. Ehsan Shakouri et al. [10] used an infrared camera to examine the thermal aspects of high-speed bone drilling of a bovine femur. The results showed the application of high rotational speeds in most cases caused increased temperature rise of the bone. Markovic et al. [12] used an infrared camera to record the temperature distribution near the hole in the bone when drilling beef ribs. The results showed that the use of surgical drill guides resulted in a higher local temperature than was the case for conventionally drilled holes, but the temperature did not exceed the threshold temperature for osteonecrosis. Gupta et al. [13] measured the temperature during the drilling of pig cortical bone using an embedded thermocouple. The results showed that a diamond-coated hollow tool could reduce significantly the drilling temperature, compared to the use of a conventional twist drill and that the temperature decreased as the radial distance around the drilled hole was increased.

However, experimental measurements of the temperature of cortical bone drilling do not provide adequate information. During the drilling process, the highest temperature often

✉ Qingchun Zheng  
zhengqingchunlg@126.com

<sup>1</sup> Tianjin Key Laboratory for Advanced Mechatronic System Design and Intelligent Control, School of Mechanical Engineering, National Demonstration Center for Experimental Mechanical and Electrical Engineering Education (Tianjin University of Technology), Tianjin 300384, China

<sup>2</sup> Tianjin Key Laboratory for Advanced Mechatronic System Design and Intelligent Control, Tianjin University of Technology, Tianjin 300384, China

occurs where the drill bit contacts with the material being drilled and the temperature at this location are difficult to obtain by measurement. Drilling tests conducted upon biologically active bone material have shown that the location of highest temperature occurrence, where osteonecrosis occurs, is the high-frequency region. Therefore, studies of temperature distribution during cortical bone drilling, therefore, are extremely useful for improving medical bone surgery.

Nowadays, numerical methods [14–16] and analytical methods [17, 18] are used to develop theoretical models of temperature distribution during machining. With the application of computer technology, simulation has been used to study the temperature distribution during drilling processes. Many scholars have used numerical methods to simulate the temperature distribution and the results were comparable to those obtained experimental tests [19, 20]. However, numerical methods also have some shortcomings. For example, there are defects in the simulation of the temperature fields of composite materials, due to limitations in parameter settings, and the numerical method cannot explain accurately the theoretical mechanisms within the system. Analytical methods can make up for this deficiency, so the analytical approach also has been applied by researchers.

Li et al. [21] analyzed the heat of drilling a laminated CFRP/Ti structure and established a temperature field model for the composite according to the Fourier heat conduction law and solved the model using the finite element method. The accuracy of the temperature field distribution within the CFRP/Ti laminated structure then was verified with experimental test data. Tauscher et al. [22] proposed an analytical temperature prediction model that used the torque signal from the drilling process to model the heat production of the drill itself. It was found that the temperature elevation could be predicted using only the torque signal from the drilling process.

In the present paper, the heat conduction differential equation during the process of cortical bone drilling is deduced, and the single-value condition of the solution is discussed. According to the heat source method, the temperature distribution of a stationary point heat source, and modeling of the temperature distribution of the moving point heat source can be solved. Verification experiments were conducted to verify the temperature distribution prediction model, which then can be used to control better drilling conditions during robot-assisted surgeries.

## Methodology

### Prediction model for temperature distribution of cortical bone drilling

#### Heat source analysis of the cortical bone drilling process

Experimental tests have shown that the axial forces from the main cutting edge and the chisel edge account for 97% of

the total axial force during drilling, with a torque of approximately 90% [23]. The shear deformation and the friction during the bone drilling is the most important causes of heat generation, in which more than 95% of the work consumed in drilling is converted into heat [24]. Therefore, the drilling heat source in the process of drilling cortical bone comes mainly from the two primary cutting edges and the chisel edge contact with the cortical bone [25]. This part of the heat source is defined as Q1, and the rest of the main cutting edge of the twist drill is mainly guided. The heat generated is much less than Q1, which we define as Q2 (as shown in Fig. 1). Q1 and Q2 are the regions that the heat is transferred to the cortical bone, so Q1 and Q2 are regarded as the sources of temperature change.

Thus, the heat during drilling can be obtained by the Law of Conservation of Energy:

$$Q = Q_1 + Q_2 \approx Q_1 = F_z \cdot v_f + M \cdot \omega \quad (1)$$

where  $F_z$ ,  $v_f$ ,  $M$ , and  $\omega$  are the axial force, feed rate, torque and angular velocity in cortical bone drilling, respectively.

### Establish the prediction model for the cortical bone drilling temperature distribution

During the cortical bone drilling process, the temperature field is in an unstable condition. As the drill continues to feed, the temperature continues to rise. According to the law of conservation of energy and the Fourier formula, the three-dimensional and unstable heat conduction partial differential equations were established on the Cartesian coordinate system, as shown in the following equation:

$$\rho c \frac{\partial T}{\partial t} = k \left( \frac{\partial^2 T}{\partial x^2} + \frac{\partial^2 T}{\partial y^2} + \frac{\partial^2 T}{\partial z^2} \right) + q_v \quad (2)$$

where  $q_v$  is the heat flux density of the heat source and  $T$  is the relative temperature rise.  $\rho$ ,  $c$  and  $k$  are the density, the specific heat capacity and the heat transfer coefficient of the material.

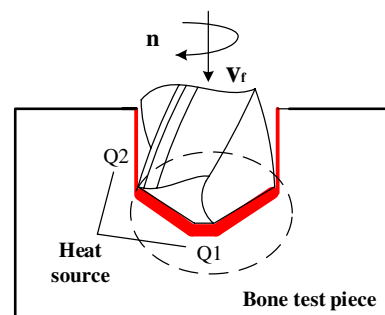


Fig. 1 Distribution of drilling heat source

The heat source during the process of drilling cortical bone is conical and, due to the complexity of the drill structure, it is difficult to capture the thermal effect of the drill. The heat source model, therefore, was simplified into a disk heat source that moves from top to bottom over time, combined with the main source of heat [26]. A fixed coordinate system on the workpiece and a moving coordinate system along the heat source of the disk were established. The center of the drilled hole was selected as the coordinate origin, as shown in Fig. 2. The circular heat source movement track is from the first drill contact on the workpiece to the hole is completely drilled, as shown in Fig. 2, from side A to side B.

The combined heat transfer control equations for cortical bone drilling in the fixed coordinate system O-xyz are as follows:

$$\rho c \frac{\partial T}{\partial t} = k \left( \frac{\partial^2 T}{\partial x^2} + \frac{\partial^2 T}{\partial y^2} + \frac{\partial^2 T}{\partial z^2} \right) \quad (3)$$

where  $T$  is the temperature rise value in the cortical bone caused by the moving heat source, which is a function of time and space. The starting time is ( $t=0$  s), when the temperature rise value is  $T=0$ .

The object studied is the internal temperature field of the workpiece, so boundary convection was not considered. With the exception of the heat source loading surface, the remaining surfaces were insulated and boundary

conditions and drilling temperature field model diagrams are shown in Fig. 3.

According to Fig. 3, the boundary conditions are as follows [27]:

$$\text{Heat source loading surface: } -k \frac{\partial T}{\partial z} = q(x, y, z, t) \quad (4)$$

$$\text{The remaining surfaces: } -k \frac{\partial T}{\partial n} = q(x, y, z, t) = 0 \quad (5)$$

The three-dimensional partial differential equation for the temperature rise can be transformed into a one-dimensional temperature rise solution in three directions, according to the separation variable method [26]. Then, using the principle of linear superposition, the temperature rise solutions in three directions can be superimposed and the temperature rise solution of the three-dimensional partial differential equation is obtained. Equations (2) and (3) can be expressed as:

$$T(x, y, z, t) = T_x(x, t)T_y(y, t)T_z(z, t) \quad (6)$$

where  $T_x(x, t)$ ,  $T_y(y, t)$ ,  $T_z(z, t)$  represent a one-dimensional temperature rise solution in three directions  $x, y, z$ .

In the X direction, according to the heat source method, the temperature distribution  $T_x(x, t)$  of the infinite body  $x' (-\infty < x' < +\infty)$  whose initial temperature is  $F(x')$  is as follows:

$$T_x(x, t) = \frac{1}{(4\pi\alpha t)^{1/2}} \int_{-\infty}^{+\infty} F(x') e^{-(x-x')^2/4\alpha t} dx' \quad (7)$$

where  $\alpha = k/\rho c$  represents the thermal diffusivity of the cortical bone.

The solution to the temperature rise in the x-direction can be calculated as:

$$T_x(x, t) = \frac{1}{(4\pi\alpha t)^{1/2}} \int_{-\infty}^{\infty} f(x') e^{-(x-x')^2/4\alpha t} dx' \quad (8)$$

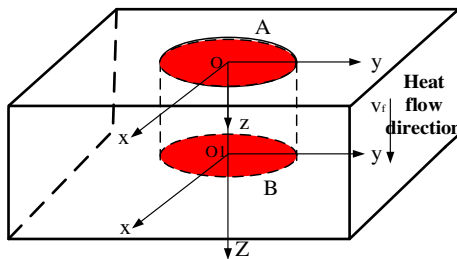
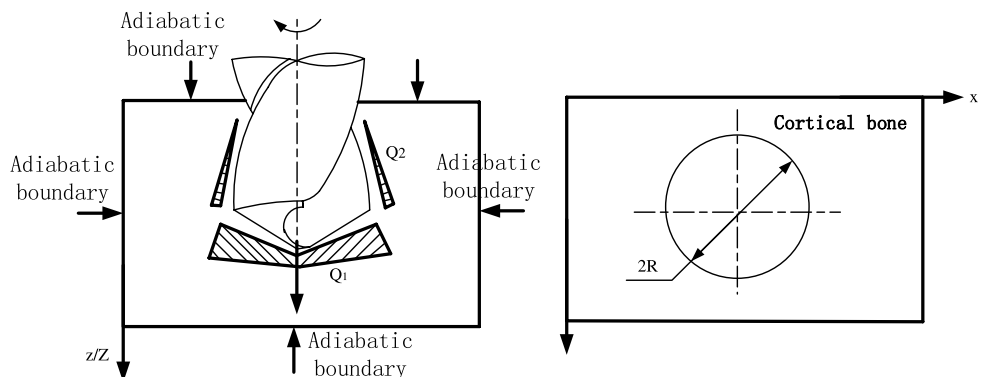


Fig. 2 Disc-shaped heat source and coordinate system

Fig. 3 Drill temperature field model and boundary conditions



According to symmetry, the temperature rise solution in the y, z-direction can be obtained as follows:

$$T_y(y, t) = \frac{1}{(4\pi\alpha t)^{1/2}} \int_{-\infty}^{\infty} f(y') e^{-(y-y')^2/4\alpha t} dy' \tag{9}$$

$$T_z(z, t) = \frac{1}{(4\pi\alpha t)^{1/2}} \int_0^{\infty} f(z') e^{-(z-z')^2/4\alpha t} dz' \tag{10}$$

Three-dimensional general solutions can be obtained by substituting the temperature rise solutions formulae, (8), (9) and (10) in the three one-dimensional directions (x, y, z) into the general solution (6):

$$T(x, y, z, t) = \frac{1}{(4\pi\alpha t)^{3/2}} \cdot \int_{-\infty}^{\infty} \int_{-\infty}^{\infty} \int_0^{\infty} f(x', y', z') e^{-\frac{(x-x')^2+(y-y')^2+(z-z')^2}{4\alpha t}} dx' dy' dz' \tag{11}$$

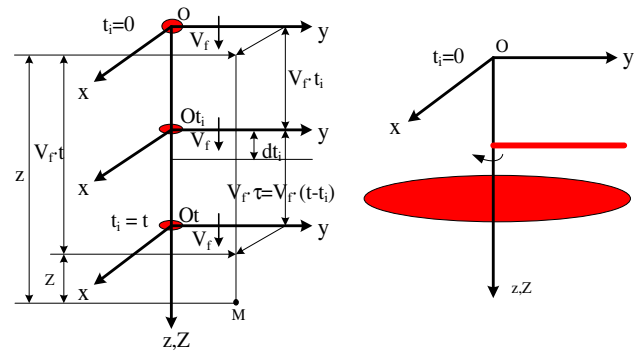
where  $f(x', y', z')$  is the initial condition of the three-dimensional general solution. The initial condition of the three-dimensional general solution is affected mainly by frictional heat and the static point heat source caused by frictional heat is  $Q_{pt}$ , according to the Dirac  $\delta$  generalized function, except that the value of the function at the heat source point is 1, the rest position function takes 0, and the temperature distribution of the static point heat source under initial conditions can be expressed as:

$$f(x', y', z') = \frac{Q_{pt}}{\rho c} \delta(x') \delta(y') \delta(z') \tag{12}$$

Substituting the temperature distribution under initial conditions into formula (11), the general solution for the temperature distribution caused by the static point heat source is as follows:

$$T(x, y, z, t) = \frac{Q_{pt}}{(4\pi\alpha t)^{3/2} \rho c} e^{-\frac{x^2+y^2+z^2}{4\alpha t}} \tag{13}$$

During the drilling process, the point heat source is moving, as shown in Fig. 4(a). The  $V_f$  is the feed rate, and the heat source moving direction is consistent with the feed direction. When the drilling  $t_i$  time has elapsed, the heat source and the moving coordinate system will move by  $V_f \cdot t_i$ . At this time, the coordinate origin of the moving coordinate system is  $Q_{ti}$ . The time parameter  $\tau(t - t_i)$ , represents the time interval from the heat source moving moment to the observation time, where  $t$  is the observation time. When the observing time is  $t$ , the origin of the moving coordinate system is  $Q_t$ , and the temperature distribution of any observation point  $M(x, y, z)$  can be obtained by the heat flux released by the heat source in an infinitesimal time interval  $d t_i$  ( $0 < t_i < t$ ). ( $Q_{pt}$ ) is expressed as shown in Eq. (14):



(a) Moving point heat source (b) Moving line heat source  
 Fig. 4 Moving heat source model and coordinate system

$$dT = \frac{q_{pt} dt_i}{(4\alpha\pi)^{3/2} \rho c} e^{-\left(\frac{x^2+y^2+(z-v_f t_i)^2}{4\alpha\tau}\right)} \tag{14}$$

Combining the relationship between the fixed coordinate system and the moving coordinate system, the influence of any observation point  $M$  by the heat source is the integral of the temperature distribution of the heat source from the initial time to the observation time  $t$ :

$$T(x, y, z, t) = \frac{q_{pt} \cdot v_f}{(16k\pi\alpha)^{3/2}} e^{-\frac{z \cdot v_f}{2\alpha}} \int_0^{\frac{v_f t}{4\alpha}} e^{\left(-w - \left(\frac{\mu^2}{4w}\right)\right)} \frac{dw}{w^{3/2}} \tag{15}$$

where  $w = \frac{v_f^2 \tau}{4\alpha}$ ;  $\mu = \frac{(x^2+y^2+Z^2)^{1/2} v_f}{2\alpha}$ .

The above formula (15) represents the temperature rise caused to the arbitrary position  $M$  when the moving point heat source feed motion and the heat source model during the drilling process is simplified to the disc-shaped heat source. A line heat source, the radius of which is  $r$ , is used to represent the surface heat source, as shown in Fig. 4(b). The heat flux density of the line heat source can be expressed as  $q_{pt} = 2qdL$ , and  $L$  represents the distance along the radial direction, which is substituted into the formula (15) to obtain:

$$dT(x, y, z, t) = \frac{2qdL \cdot v_f}{(16k\pi\alpha)^{3/2}} e^{-\frac{z \cdot v_f}{2\alpha}} \int_0^{\frac{v_f t}{4\alpha}} e^{\left(-w - \left(\frac{\mu^2}{4w}\right)\right)} \frac{dw}{w^{3/2}} \tag{16}$$

where  $\mu_i = \frac{((x-x_i)^2+(y-y_i)^2+Z^2)^{1/2} v_f}{2\alpha} x'x'$

The line integral of formula (16) gives a temperature rise solution caused by the moving disk surface heat source at any position  $M$  at any time. The temperature rise solution at this time is derived from the ideal state in which the work-piece material is infinitely substantial. In the actual drilling process, the heat source in the cortical bone material only extends in the x, y direction, and the z-axis direction extends

along the heat source feeding direction. Therefore, the workpiece material is semi-infinite in the process of cortical bone drilling. In addition, the temperature ( $T_0$ ) must be loaded in the initial state to obtain the temperature change at the point M, so the cortical bone temperature distribution prediction model at any point M can be corrected and is shown in formula (17).

$$T = \frac{2B(M\omega + F_z v_f)}{\pi R^2} dL \cdot v_f \int_0^r \left[ \int_0^\tau \frac{z \cdot v_f}{2\alpha} \left( \int_0^{\frac{v_f^2 t}{4\alpha}} e^{\left(-w - \left(\frac{\mu_z^2}{4w}\right)}\right)} \frac{dw}{w^{3/2}} \right) dy \right] dL + T_0 \tag{17}$$

$$\xi^n = \frac{\sum_{i=1}^m \left( \frac{\partial T_g(B^n)}{\partial B^n} \right)^T d^n [T_c - T_g(B^n)]}{\sum_{i=1}^m \left[ \left( \frac{\partial T_g(B^n)}{\partial B^n} \right)^T d^n \right]^2} \tag{21}$$

The iterative termination condition is  $J(B^{(n+1)}) < \epsilon$ , where  $\epsilon$  is a small positive integer.

**Determination of parameters of temperature prediction model**

From the prediction model described in the previous section, it is known that the parameters for predicting the cortical bone temperature distribution need to be calculated or measured and are the proportional coefficient B of the drilling heat transfer to the cortical bone workpiece, the drilling axial force  $F_z$ , and the torque M.

$F_z$  and M can be measured using a dynamometer (shown in Fig. 6). According to the study by Orlande, using the inverse heat conduction problem to calculate the heat partition coefficient of the cortical bone, In the present study, the conjugate gradient method [28] is used to obtain the heat distribution coefficient during the drilling process.

The least squares method was used to determine the objective function, with B as the variable:

$$J(B) = \sum_{i=1}^m (T_g(B) - T_c)^2 \tag{18}$$

where  $m$  is the number of temperature values;  $T_g(B)$  is the temperature estimate;  $T_c$  is the temperature measurement; the inversion problem is transformed into the parameter  $J(B)$  minimum, and the parameter B is optimized.

Suppose the  $n + 1$ th iteration of variable B is :  $B^{n+1} = B^n - \xi^n d^n$  (19)

where  $n$  is the number of iterations;  $\xi$  is the search step size;  $d$  is the conjugate search direction, and the direction of the fall is composed of the conjugate direction and the gradient direction.

$$d^n = \nabla J(B^n) + \chi^n d^{n-1} \tag{20}$$

where  $\nabla J(B^n)$  and  $\chi^n$  respectively represent the objective function gradient value and the conjugate coefficient of the  $n^{\text{th}}$  iteration, then the  $n^{\text{th}}$  iteration search step  $\xi^n$  can be expressed as:

**Test materials**

Previous studies have shown that [29]: pig bones are similar to human bones, both in terms of density of cortical bone and structural models of bone. Therefore, the workpiece material used in the present tests was a fresh pork bone, the cortical bone samples of the pigs which had the same age and the same position were selected. In order to ensure the accuracy of the test, the thickness of all the selected pig bone samples was about 4 mm. The surface soft tissue treatment of the pig bone sample was carried out and only the middle bone part was reserved as test work, so as to be fixed and installed. The treated cortical bone test piece is shown in Fig. 5. A 4Cr13 stainless steel medical twist drill was used.

**Equipment**

The cortical bone drilling tests were carried out on a Yongjin YCM-V65A vertical machining center. A Kistler 9129A dynamometer was used to measures thrust force and torque during drilling. The temperature at the specified location inside the cortical bone was measured using a type K thermocouple. A Fluke TiX640 infrared camera was used to monitor the temperature of the cortical bone surface. The thermal range of this camera was  $-40$  to  $1200$  °C with a thermography resolution of 307,200 pixels, the heat sensitivity of 0.03 °C and the spectral range of 7.5–14  $\mu\text{m}$ . Figure 6 is a schematic diagram of a cortical bone drilling experiment system.

**Test program**

The tests were used to confirm the accuracy of the prediction model for cortical bone drilling temperature distribution, which was described in the second section of the present paper. The test scheme for obtaining temperature changes at different times at the same position is shown in Table 1.

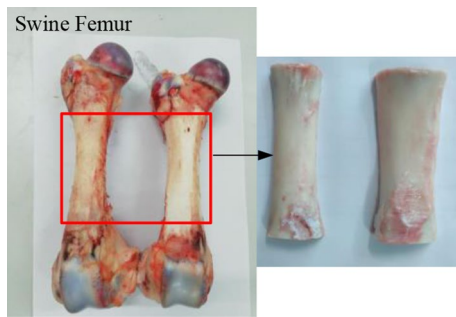


**Fig. 5** Samples of cortical bone

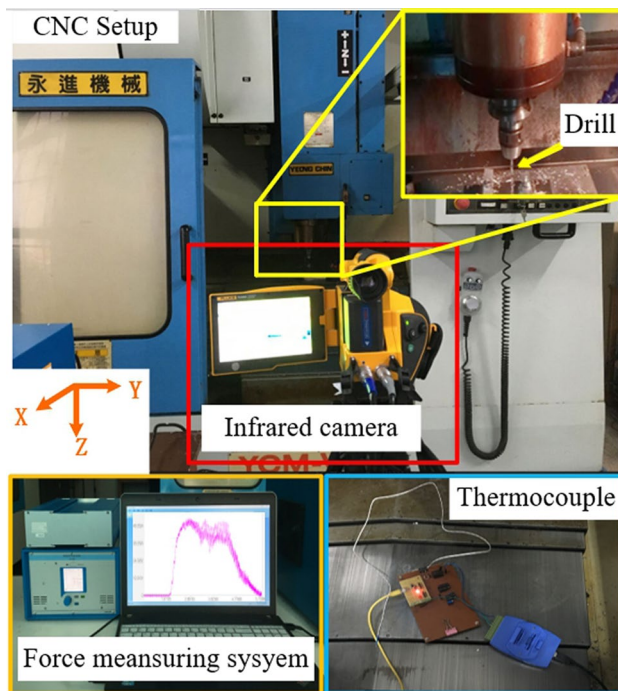


**Fig. 6** Cortical bone drilling experiment system

When the cortical bone was just drilled, the cumulative temperature was highest. In order to further verify the reliability of the model, the temperature distribution of the different radial distances of the upper surface of the cortical bone was studied under the same drilling conditions (spindle speed, feed rate, and drill diameter are 1000 rpm, 40 mm/min, 4 mm respectively), and all of the cortical bone samples have been drilled through.  $d$  was the diameter of the twist drill;  $x$  was the distance between the temperature collection point (TCP) and the wall of the cortical drilled hole (shown in Fig. 7). The test design is shown in Table 2.

The tests were carried out at room temperature (23 °C). Each set of parameters in the test was repeated three times to reduce the accidental error. After each set of drilling tests,

**Table 1** Design of temperature test changes at different measurement locations

Number	Drill diameter $d$ (mm)	Spindle speed $n$ (mm)	Feed rate $V_f$ (mm/min)	Measurement position ( $s + d/2, 0, h$ ) mm
(a)	4	1000	60	(2.5, 0, 2)
(b)	4	1000	40	(2.5, 0, 2)
(c)	4	800	60	(2.5, 0, 2)
(d)	4	800	40	(2.5, 0, 2)
(e)	3.2	1000	60	(2.1, 0, 2)
(f)	3.2	800	40	(2.1, 0, 2)

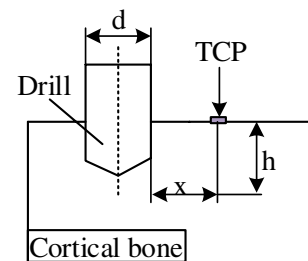


**Fig. 7** Measurement location

**Table 2** Design of temperature tests at different times

Number	Drill diameter $D$ (mm)	Measurement position ( $s + d/2, 0, h$ ) (mm)	Spindle speed $n$ (rpm)	Feed rate $f_v$ (mm/min)
1	4	(2.6, 0, 2)	1000	40
2		(2.7, 0, 2)		
3		(2.8, 0, 2)		
4		(2.9, 0, 2)		
5		(3.0, 0, 2)		

the medical twist drill was replaced to avoid the influence of the temperature accumulation on the drill.

## Results and discussion

### Model loading parameters $F_z$ and $M$

During the cortical bone drilling process, a Kistler 9129A dynamometer was used to record the axial force and torque. The results are shown in Table 3. The energy distribution coefficient for drilling cortical bone was solved according to formulae (18)–(21), and the value was 11.7% as calculated by Matlab programming.

## Verification of the temperature distribution prediction model in the same location

According to the experimental design, the cortical bone drilling tests were carried out, the temperature was recorded, and the simulation model obtained under the same drilling conditions was compared with the results from the prediction model in order to verify the accuracy of the temperature prediction model. According to the temperature prediction model formula (17), the predicted temperature value was calculated by Matlab. The test values and estimated values of cortical bone temperature change with time under different drilling conditions are shown in Fig. 8.

Figure 8 shows the experimental test values (TV) and the calculated simulation values (SV) under six drilling conditions. The thermocouple was mounted at  $(d/2 + 0.5, 0.2)$  mm where  $d$  was the diameter of the medical twist drill. It was confirmed that the experimental test and simulation estimated results were similar, and the simulation values is basically consistent with the values obtained by the prediction models established by Maani Nazanin [30] and Lee JuEun [31]. So the model was demonstrated to predict accurately the temperature field during the cortical bone drilling process. The experimental test design is summarized in Table 1. The test values and simulation values of the maximum temperature under different drilling conditions are shown in Table 4. When the feed rate was 60 mm/min, and the spindle speed was 1000 rpm and the drill diameter was 4 mm, the measured temperature was up to 56.8 °C. Furthermore, the maximum relative error (RE) between the test measurements and the simulation results was 13.6%. When the rotational speed of 1000 rpm has been used, the values obtained in the experiments are larger than the simulation values. This difference is due to the negligence of the heat generated by the friction between the chip and the hole wall during the bone drilling operations. The energy distribution coefficient of the bone is not constant, which depends on the drilling conditions (the rotational speed and the feed rate). This coefficient would decrease with the increase in the feed rate. In this study, with the increase of feed rate, the change

of coefficient is very slight because of the small range of the feed rate change (40–60 mm/min). So the reduction of coefficient was ignored. This is the reason for the deviation between TV and SV at a high feed rate (60 mm/min). According to the test measurements and simulation results, the temperature changes gradually increase with time. The temperature rises rapidly around the third second. According to the study results of groups (a), (b) and groups (c), (d), within the scope of the study, the temperature increased with increase in the spindle speed. The results of tests (a) (d) and (b) (c) showed that the temperature was higher with higher feed rates; The results of tests (b) (f) and (d) (e) indicated that the larger the drill diameter, the higher the temperature.

During the cortical bone drilling process, the heat source will continue to release heat. The semi-enclosed processing environment and the low thermal conductivity of the cortical bone make heat dissipation lower than heat production. The drilling heat continues to accumulate and the temperature of the measurement point continues to rise. With drill movement during the drilling process, the heat source and the temperature measurement point are close to each other. This can explain why all the temperature curves in Fig. 8 rise rapidly around the third second. When the heat source continues to move with drill movement, the distance between the heat source and the temperature measurement point increases, and the temperature rise is slow, so the rate of increase gradually decreases.

Drilling parameters are the main factors that affect the temperature rise of cortical bone drilling area. First, as the rotational speed increases from 800 rpm to 1000 rpm, an increase in the number of contacts between the chip and the wall results in an increase in friction. Since most of the friction energy is converted into heat energy, it is a reasonable result that the temperature increases as the rotational speed increases. Second, the effect of the feed rate on the temperature rise is complex. On one hand, the higher feed rate result in more material being removed per second, which in turn produces more heat in the bone. On the other hand, the improved heat dissipation in drilling zone was caused by the improvement of the chip evacuation rate and the reduction in heat transfer time. In the range of feed rate (40–60 mm/min) selected in this paper, heat generation plays a leading role compared with the improved heat dissipation conditions. As a result, the temperature of the cutting area of cortical bone increases slightly with the feed rate from 40 mm/min to 60 mm/min. Third, the heat generation is increased with the diameter, but the temperature rise is not obvious. The possible explanation might be that the diameter of the drill is  $\leq 4$  mm, the temperature change was not obvious with small changes in diameter. The results of our study are generally consistent with the results of most other researchers [3, 30–33].

**Table 3** Axial forces and torques under different drilling conditions

Spindle speed $n$ (rpm)	Feed rate $f_v$ (mm/min)	Diameter $d$ (mm)	Axial force $F_z$ (N)	Torque $M$ (N m)
1000	60	4	$30.0 \pm 0.75$	$0.10 \pm 0.002$
1000	40	4	$29.2 \pm 0.60$	$0.10 \pm 0.003$
1000	60	3.2	$29.6 \pm 0.58$	$0.11 \pm 0.002$
800	60	4	$31.7 \pm 0.71$	$0.13 \pm 0.002$
800	40	4	$31.2 \pm 0.92$	$0.14 \pm 0.001$
800	40	3.2	$33.3 \pm 0.85$	$0.17 \pm 0.004$

**Fig. 8** Test values (TV) and simulation values (SV) of cortical bone temperature

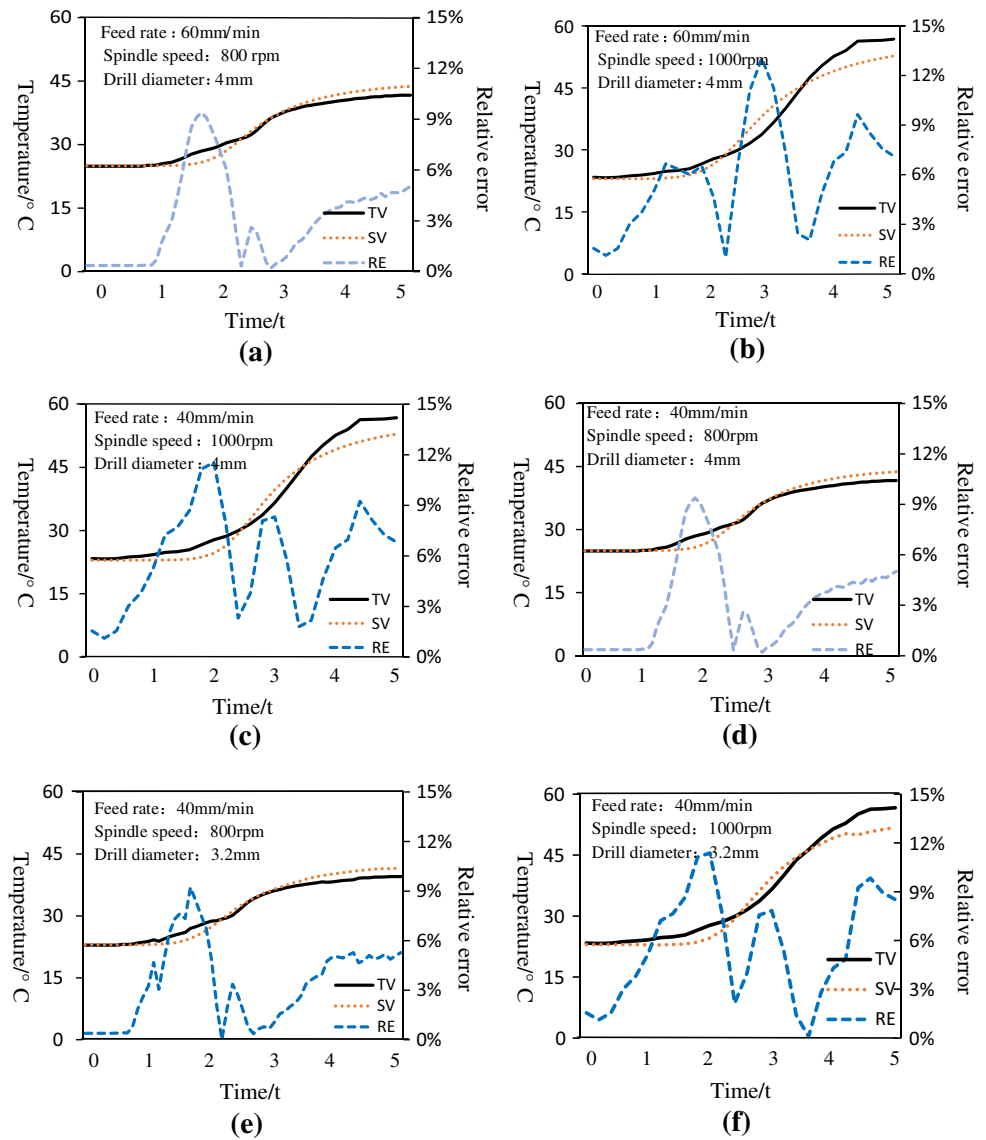


**Table 4** Maximum temperature values of test values (TV) and simulation values (SV)

Number	Maximum temperature (°C)		Maximum error (%)
	TV	SV	
(a)	39.7 ± 0.93	41.8	5.3
(b)	56.8 ± 1.06	52.7	7.2
(c)	56.3 ± 0.85	52.3	7.0
(d)	39.1 ± 0.88	39.8	1.8
(e)	39.5 ± 0.74	41.6	5.3
(f)	56.6 ± 1.23	51.8	8.5

**Temperature distribution prediction model verification for different measurement locations at the same time**

The experimental test data and the calculated simulation values for the different radial temperatures of the upper surface of the cortical bone are shown in Fig. 9. The maximum error was 3.5%. The predictive model can estimate the temperature at different radial positions. It can be seen from Fig. 9 that as the radial distance increases, both the predicted value and the measured test value had the same tendency to change, and the temperature of the cortical bone decreased



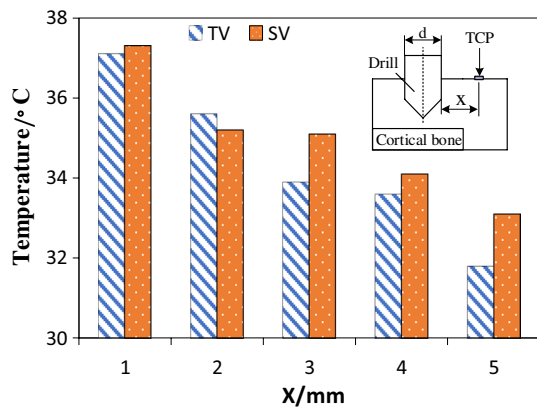


**Fig. 9** Temperature values of different radial distances X

as the radial distance was increased. Because the heat source is in the drilling area during the drilling process, the temperature accumulation is greater near the drilling area. The low thermal conductivity of the cortical bone causes hysteresis in the diffusion of the drilling temperature, so the temperature change of the cortical bone away from the drilled hole is low.

## Conclusions

The heat source model and its motion during cortical bone drilling were analyzed during the present study, and the temperature distribution of the static point heat source was obtained by the heat source method. Based on this, the temperature distribution of the moving point heat source was derived. The energy partition coefficient of cortical bone was calculated using the conjugate gradient method and the calculated result was 11.7%. The conclusions from the investigation can be summarized as follows:

1. Comparing the measured temperature values and predicted values of the bone drilling tests under different conditions, the maximum differential between the test measurements and simulation results was 13.6%, and it was concluded that the model could predict temperature changes during the cortical bone drilling process.
2. Increases in spindle speed, feed rate, and drill diameter will lead to an increase in cortical bone temperature. However, changes in drill diameter have less influence on the temperature than do the other parameters.
3. The established prediction model can provide the possibility of controlling the temperature during the operation by controlling the spindle speed and feed rate.

**Funding** This study was funded by the Key Fund of Tianjin Natural Science Foundation of China (Grant No.15JCZDJC32800) and the National Natural Science Foundation of China (Grant No.11672208, Grant No.81741141).

## Compliance with ethical standards

**Conflict of interest** The author(s) declared no potential conflicts of interest with respect to the research, authorship, and/or publication of this article.

**Ethical approval** This article does not contain any studies with human participants or animals performed by any of the authors.

**Informed consent** Informed consent was obtained from all individual participants included in the study.

## References

1. Augustin G, Davila S, Udiljak T et al (2012) Temperature changes during cortical bone drilling with a newly designed step drill and an internally cooled drill I [J]. *Int Orthop* 36(7):1449
2. Ke X, Qun X, Lin-hong JI et al (2009) Influence of a minimally invasive bone drill cutting parameters on cutting forces and temperature [J]. *Mach Des Manuf* (2):264–266
3. QingYun Z (2014) Finite element analysis and experimental research of cortical bone drilling performance based on ABAQUS [D]. Tianjin University of Technology, Tianjin
4. Eriksson AR, Albrektsson T, Grane B, McQueen D (1983) Thermal injury to bone. A vital-microscopic description of heat effects [J]. *Int J Oral Surg* 11:115–121
5. Eriksson R, Albrektsson T (1983) Temperature threshold levels for heat-induced bone tissue injury: a vital-microscopic study in the rabbit [J]. *J Prosthetic Dent* 50:101–107
6. Allan W, Williams ED, Kerawala CJ (2005) Effects of repeated drill use on temperature of bone during preparation for osteosynthesis self-tapping screws [J]. *Br J Oral Maxillofac Surg* 43:314–319
7. Matthes M, Pillich DT, El Refaee E (2018) Heat generation during bony decompression of lumbar spinal stenosis using a high-speed diamond drill with or without automated irrigation and an ultrasonic bone-cutting knife: a single-blinded prospective randomized controlled study [J]. *World Neurosurg* 111:72–81
8. Shakouri E, Ghorbani M (2020) Nezhad. An in vitro study of bone drilling: infrared thermography and evaluation of thermal changes of bone and drill bit [J]. *Phys Eng Sci Med* 43(1):247–257
9. Shakouri E, Mirfallah P (2019) Infrared thermography of high-speed grinding of bone in skull base neurosurgery [J]. *Proc Inst Mech Eng Part H: J Eng Med* 233(6):648–656
10. Shakouri E, Nezhad MG, Ghorbani P, Khosravi-Nejad F (2020) Investigation of thermal aspects of high-speed drilling of bone by theoretical and experimental approaches [J]. *Phys Eng Sci Med* (prepublish)
11. Omar NA, McKinley JC (2018) Measurement of temperature induced in bone during drilling in minimally invasive foot surgery [J]. *Foot* 35:63–69
12. Aleksa M, Zoran L, Tijana M et al (2016) Effect of surgical drill guide and irrigants temperature on thermal bone changes during drilling implant sites: thermographic analysis on bovine ribs [J]. *Hum Vet Med* 73(8):744–750

13. Gupta V, Pandey PM, Mridha AR (2017) Effect of various parameters on the temperature distribution in conventional and diamond coated hollow tool bone drilling: a comparative study [J]. *Procedia Eng* (04):74
14. Wu J, Han RD (2009) A new approach to predicting the maximum temperature in dry drilling based on a finite element model [J]. *Manuf Process* 11:19–30
15. Ozcelik B, Bagci E (2006) Experimental and numerical studies on the determination of twist drill temperature in dry drilling: a new approach [J]. *Mater Des* 27:920–927
16. Bagci E, Ozcelik B (2006) Finite element and experimental investigation of temperature changes on a twist drill in sequential dry drilling [J]. *Int J Adv Manuf Technol* 28:680–687
17. Heydari H, Kazerooni NC, Zolfaghari M (2018) Analytical and experimental study of effective parameters on process temperature during cortical bone drilling [J]. *J Eng Med* 232(9):871–883
18. Shakouri E, Sadeghi MH, Maerefat M (2014) Experimental and analytical investigation of the thermal necrosis in high-speed drilling of bone [J]. *J Eng Med* 228(4):330–341
19. Tu Y-K, Tsai H-H et al (2008) Finite element simulation of drill bit and bone thermal contact during drilling [J]. *Int Conf Bioinform Biomed Eng* (08):1268–1271
20. Jian W (2010) Basic research on the related technologies of drilling typical difficult-to-machine materials [D]. Harbin Institute of Technology, Harbin
21. Li Jian, Li Yuan, Zhang Kai Fu, et al (2016) Research on temperature distribution in drilling of CFRP/Tistacks [D]
22. Tauscher S, Fuchs A, Baier F, Kahrs LA, Ortmaier T (2017) High-accuracy drilling with an image guided light weight robot: autonomous versus intuitive feed control [J]. *Int J Comput Assist Radiol Surg* 12(10):1763–1773
23. RiYao C (2005) Principles of metal cutting [M], 2nd edn. Mechanical Industry Press, Beijing, pp 1–228
24. Ramulu M (1997) Machining and surface integrity of fibre-reinforced plastic composites [J]. *Sadhana* 22(3):449–472
25. Amewoui F, Le Coz G, Bonnet A-S, Moufki A (2020) An analytical modeling with experimental validation of bone temperature rise in drilling process [J]. *Med Eng Phys* 84:151–160
26. Hu HP (2010) Heat conduction theory [M]. China Science and Technology Press, AnHui, pp 9–250
27. Zhu GuoPing (2013) Study on drilling temperature field of unidirectional carbon/epoxy composites [D]
28. Hong Tan W (2005) Application of conjugate gradient method to two-dimensional inverse convective heat transfer problem [J]. *J Astron Metrol Measure* (04):25–27 +40
29. Miller ER, Ullrey DE (1987) The pig as a model for human nutrition [J]. *Annu Rev Nutr* 7:361–382
30. Nazanin M, Kambiz F, Mohammad H (2014) A model for the prediction of thermal response of bone in surgical drilling [J]. *J Thermal Sci Eng Appl* 6(4):041005
31. JuEun L, Yoed R, Burak OO (2011) A new thermal model for bone drilling with applications to orthopaedic surgery [J]. *Med Eng Phys* 33(10):1234–1244
32. Alam K, Hassan E, Bahadur I (2015) Experimental measurements of temperatures in ultrasonically assisted drilling of cortical bone [J]. *Biotechnol Biotechnol Equip* 29:753–757
33. Gupta V, Pandey PM, Mridha AR, Gupta RK (2017) Effect of various parameters on the temperature distribution in conventional and diamond coated hollow tool bone drilling: a comparative study [J]. *Procedia Eng* 184:90–98

**Publisher's Note** Springer Nature remains neutral with regard to jurisdictional claims in published maps and institutional affiliations.